Robust active noise control in a car cabin: evaluation of achievable performances with a feedback control scheme

Paul Loiseau, Philippe Chevrel, Mohamed Yagoubi, Jean-Marc Duffal

Robust active noise control in a car cabin: evaluation of achievable performances with a feedback control scheme

Paul Loiseau[a,*], Philippe Chevrel[a], Mohamed Yagoubi[a], Jean-Marc Duffal[b]

[a] *IMT-Atlantique, LS2N (Laboratoire des Sciences du Numérique de Nantes), UBL, 44307 Nantes, France*
[b] *Renault SAS, 78288 Guyancourt, France*

Abstract

The application dealt with in this paper is the active attenuation of broadband noise (produced by the tire/road contact) in a car cabin, using only a feedback control scheme (1-DOF (one degree of freedom)). The objective of the proposed control methodology is to evaluate achievable performances according to the frequency bandwidth in which attenuation is desired. This is investigated numerically, by seeking a multi-input multi-output (MIMO) active noise control solution that reaches the best attenuation level, under explicit robustness constraints. The paper aims to i) formalize the underlying optimization problem including performance and robustness indicators as well as industrial constraints, ii) perform an effective MIMO identification, and iii) provide an *a priori* control structure and then proceed to direct optimization of some meaningful parameters using a well-suited nonsmooth optimization solver. Finally, the simulation and experimental results obtained following the proposed methodology are shown and discussed.

Keywords: Active noise control, Broadband noise attenuation, Automotive control, Multi-objective control, Robust control

1. Introduction

The principle of active noise control (ANC), which consists of attenuating an annoying noise with an anti-noise of the same magnitude and shifted by half a wavelength, was described for the first time in the 1930s in two patents [1, 2]. In practice, the level of difficulty associated with an ANC problem varies. For example, ANC in an open-ended duct, involving propagating waves, can be achieved by means of a 2-DOF control scheme (*i.e.* a pre-compensation coupled with a feedback control) since the disturbing noise can be measured both upstream of the actuator and at the end of the duct [3, 4, 5, 6]. In contrast, applications of ANC in enclosures need to deal with stationary waves. Good performances can still be obtained if the actuators and sensors are co-located, such as in active headphones or active headrest applications [7, 8, 9]. The difficulty increases when the actuators and sensors are not co-located, such as in the problem of attenuating engine noise at the position of passengers' ears in a car cabin using door loudspeakers. However, an advantage in this particular case is that the engine noise has a line spectrum whose frequency can be directly deduced from the measure of the engine speed [10, 11, 12].

In the present paper, the considered application consists of attenuating low frequency broadband noise in a car cabin. The main source of this broadband noise is the road noise, which is generated by the tire/road contact. In this case, obtaining a measure of the perturbation is generally not feasible due to industrial costs and integration constraints. Moreover, the attenuation must be obtained not at some isolated frequencies but over a (wide) frequency range. The authors previously proposed a single-input single-output (SISO) robust multi-objective ANC control synthesis in [13] and an overall methodology to compare the best achievable performances according to the number of sensor(s) and actuator(s) used [14]. The current paper pursues the latter objective by considering the needs of the automotive industry, using only feedback and exploiting the available microphones and loudspeakers. Hence, this paper is an improved and extended version of the authors' initial work presented in [15]. In particular, a far more complete overview of possible indicators is provided. The possibilities and limitations of all these indicators are fully discussed and illustrated with concrete results. This discussion, which is central when dealing with the evaluation of multivariable ANC solutions or aiming to compare multivariable ANC strategies, is missing in the current literature. Then, improved and additional results are provided and analyzed in more depth. The results presented in [15] were encouraging, but did not enable any conclusion about the achievable performances on the vehicle platform; this was pointed out as a perspective. In the present paper, this remaining problem is solved and clear conclusions are given with regard to the vehicle platform. Finally, this paper is more detailed and gives a more pre-

*Corresponding author
Email address: paul.loiseau@imt-atlantique.fr (Paul Loiseau)

cise overview of the whole study conducted by the authors.

Solving the considered ANC problem requires two crucial points to be addressed: i) obtaining an acoustic model that reproduces finely the system behavior over a sufficiently large frequency range and ii) defining a generic control synthesis problem faithfully reflecting the industrial constraints.

Let us first consider how to obtain a model of the system. A direct way to derive an acoustic model is to solve the wave equation with the appropriate boundary conditions. This leads to a model of infinite dimension, which can generally be reduced to a finite dimension model by keeping only the predominant acoustic modes. However, this approach suffers from several drawbacks. First, purely acoustic models usually fail to reproduce the system behavior and coupling with structural dynamics must generally be taken into account (see, for example, [12, 16]). Secondly, realistic boundary conditions are usually complex to formalize and the simplifications made are the main source of error for analytical models [16]. In addition, there is no systematic technique for estimating the damping. For these reasons, in this paper we opt for the identification approach.

Most methods used to identify an acoustic model for ANC (LMS, RLS, ARMA, ARMAX, OE) proceed in the time domain and look for discrete time models [17, 18]. Another approach presented in [19] is to minimize the distance between the measured frequency response of the system and an adequate transfer function. This method is effective for narrow frequency ranges, but encounters difficulties for increased system dimensions and model order. Lastly, a method commonly used in ANC applications is subspace identification [20, 21, 22]. This approach identifies either a continuous or a discrete time model, from either frequency or time domain data. It is not based on parametric optimization and consequently does not need any particular parametrization for the model. It does not suffer from the convergence problems encountered by iterative algorithms. Moreover, models are obtained directly in the state space and the frequency approach is well suited for systems with a high modal density and poorly damped modes [20].

In the present work, the subspace approach operating in the frequency domain was found to be one effective method of reproducing the system behavior over a large frequency range [20-1000] Hz. This large range is needed to achieve broadband attenuation safely with a feedback control scheme. In fact, as formalized by the Bode integral relation, the attenuation on the sensitivity function at certain frequencies is obtained at the price of an amplification at other frequencies. (This phenomenon is typically referred to as the "waterbed effect".) Thus, a feedback controller will contain dynamics outside the target frequency range and the system behavior must be known over a wide range, which unfortunately results in high order models. As in [13, 14], the subspace method is used to obtain a continuous time model from frequency domain data (see [23, 24] for details on the corresponding identification algorithm). The authors also tested some alternative approaches such as the one based on Loewner matrices [25]. To date, They have led to results similar to those obtained with the subspace approach.

Concerning the control problem itself, the proposed control methodology aims to evaluate achievable performances depending on the frequency bandwidth in which attenuation is desired. It also concentrates on robustness, which is not the case of most existing adaptive control strategies. In fact, the extensive literature dedicated to this subject refers to the FxLMS adaptive control strategy and its numerous variants [12, 26, 27, 28], whose robustness is not yet fully established. Elements of a comparison between the FxLMS strategy and the approach proposed in this paper can be found in [29]. This is by no means the purpose of the current paper. However, it can be noted that the results obtained in [29] in the SISO case show that the present strategy is better suited to evaluate achievable performances accurately.

Other approaches deal with robust control strategies, such as LQG [30, 31] or standard $\mathcal{H}_\infty$ [21, 32]. Based on convex optimization problems, these approaches are certainly tractable and offer interesting solutions to some specific ANC problems. However, for broadband attenuation problems, control engineers are faced with high order models and highly constrained control problems, often leading to unsolvable problems or to solutions far from realistic specifications (too conservative).

The alternative approach proposed in this paper aims to formulate a multi-objective control problem, by specifying performance and robustness explicitly. Clearly, the underlying optimization problem is both non-convex and non-smooth. However, powerful non-smooth solvers now exist that enable a rapid convergence to local optima. Combined with an appropriate initialization step, they can solve the problem without pessimism.

The paper is organized as follows: first, the ANC problem and the experimental demonstrators are presented in Section 2. Then, an overview of performance and robustness indicators for ANC applications is given in Section 3. Section 4 describes the identification process used to obtain an acoustic model for the two demonstrators considered. Then, the proposed control strategy is introduced in Section 5. Finally, Section 6 is dedicated to analyzing the results and discussing achievable performances, while the conclusion summarizes the content and contributions.

2. Problem description

2.1. Automotive context and industrial specifications

Inside a car cabin, permanent noise mainly comes from three sources :

- aeroacoustic noise;
- engine noise;

- road noise.

Aeroacoustic noise, generated by the air flow around the vehicle, mainly affects high frequencies, while engine noise and road noise (generated by the tire/road contact) intervene at low frequency. To date, noise reduction inside cars has essentially been achieved through passive treatments. These technologies are based on a judicious adjustment of the mass, stiffness and damping of the different components of a car in order to reduce the noise either directly at its source or during its transmission to the cabin. Passive technologies provide a good level of comfort, especially when considering high frequency noise such as aeroacoustic noise. However, for low frequency noise such as engine and road noise, they require a large addition of weight. In order to meet challenging fuel consumption constraints, car makers are therefore looking for alternative technologies that reduce low frequency noise without a negative impact on consumption.

ANC solutions, which are essentially efficient at low frequencies, are seen as a promising alternative and some are already used to reduce engine noise [10, 11, 12]. This noise has a line spectrum whose harmonics move according to the engine speed. By measuring the engine speed, the frequencies of the different harmonics are easily identified and those that emerge clearly from the background noise are reduced.

After the successful application of ANC to engine noise, the next step is to consider road noise reduction. Contrary to engine noise, road noise has a broadband spectrum coming from four (potentially independent) sources (the wheels). Moreover, the transmission path between the tires/road excitation and the cabin is complex. The first solutions proposed for the ANC of road noise use a set of accelerometers attached to the vehicle suspension and bodywork in order to measure the excitation, and a set of microphones inside the cabin in order to measure the resulting noise [27]. The proposed control strategy then involves both a feedforward and a feedback action and leads to significant noise reduction when the measures from the accelerometers are reliable. Unfortunately, the coherence between the accelerometer signals and the cabin noise is generally poor. Thus, obtaining a reliable measure of the tire/road excitation requires numerous accelerometers. The cost of these additional sensors is the main reason why car makers are searching for alternatives.

The specifications considered here for an industrial solution require the use of the same sensors and actuators as are used for engine noise reduction, *i.e.* the four door loudspeakers and a set of microphones. The objective of the present work is thus to investigate the achievable performances with these constraints, *i.e.* using feedback control only (no anticipation through feedforward is possible).

2.2. Vehicle demonstrator

A diagram of the vehicle demonstrator that supports this work is presented in Fig. 1. It is a Renault Scenic whose audio system has been modified in order to test ANC applications. As specified above, the ANC device is composed of the four serial door loudspeakers and three microphones placed in the roof. It is monitored by an Autobox DS 1103 (dSPACE). The sampling frequency used is 2048 Hz and the microphone signals are filtered with an anti-aliasing filter whose cut-off frequency is 800 Hz.

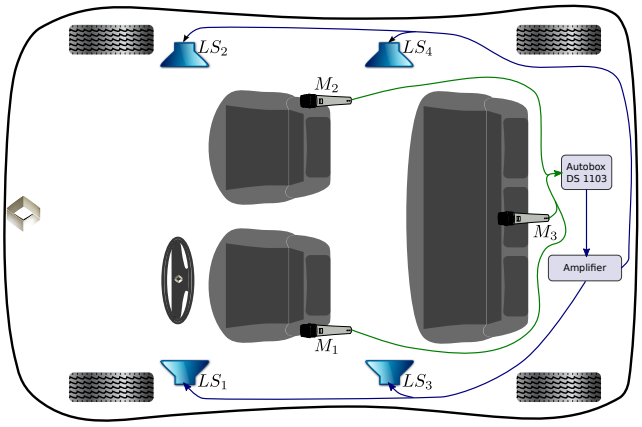

Figure 1: Vehicle demonstrator

Fig. 2 presents some frequency responses measured on the vehicle (from loudspeakers LS_1 and LS_4 and microphone M_3). Each transfer contains numerous modes. A large difference in the magnitude level can be noticed. Front/rear (or rear/front) crossed transfers (for instance $LS_1 \rightarrow M_3$) have a lower magnitude level than rear/rear (or front/front) transfers (for instance $LS_4 \rightarrow M_3$) except below 80 Hz where the magnitude level and the modal density is bigger for crossed transfers. This difference in gain leads to some difficulties during the identification process presented in the following.

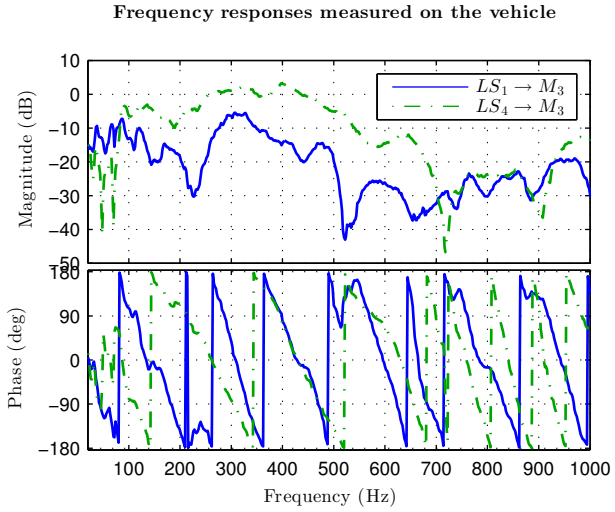

Figure 2: Frequency responses measured on the vehicle

2.3. Control problem position and notations

The 1-DOF control problem is described in Fig. 3. In this block diagram, the disturbance source (the tire/road excitation) is named u_p and the resulting noise in the car cabin is y_p. G_p is the transfer between u_p and y_p. In the ANC literature, it is generally called the primary path. The signal $u = u_s$ is the control input applied to the loudspeakers, y_s is the resulting anti-noise and G_s (the secondary path) is the MIMO transfer between the loudspeakers (LS_1, ..., LS_4 in Fig. 1) and the microphones (M_1, ..., M_3). The actual noise in the car cabin e is the sum of the noise y_p and the anti-noise y_s. $y = e$ is the only measured output and the block K is the controller.

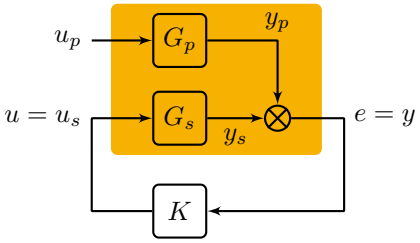

Figure 3: Control problem

As mentioned above, no measure of u_p is available and so a pure feedback control structure must be used. Furthermore, G_p is unknown and no model is available for the signal y_p (output disturbance). Obtaining such a model would involve spectral factorization [33, 34]. Unfortunately, finding a representative spectrum of the noise is difficult due to the large number and variability of the parameters involved (road surface, vehicle load, temperature, etc.). This is not considered in the present work.

2.4. LS2N Box demonstrator

Before considering the vehicle application, the ANC problem presented above was first studied in the simplified acoustic environment described in Fig. 4. This demonstrator offers a fully mastered experimental environment, which facilitates early investigations.

The enclosure is made of plywood with a Plexiglas top. It is a $1.2 \times 0.3 \times 0.25\ m^3$ volume. It has one predominant dimension, which results in a 1D acoustic field at low frequency. One side of the enclosure is biased to avoid the first longitudinal acoustic mode being too pronounced. Its simple shape enables a rapid understanding of the enclosure's acoustic field through very basic models, such as that of a closed rectangular cavity (presented in [35] page 153). At the same time, the frequency responses of the different transfers between loudspeakers and microphones contain several modes at low frequency and are close to vehicle complexity (see Fig. 5). As the plywood enclosure

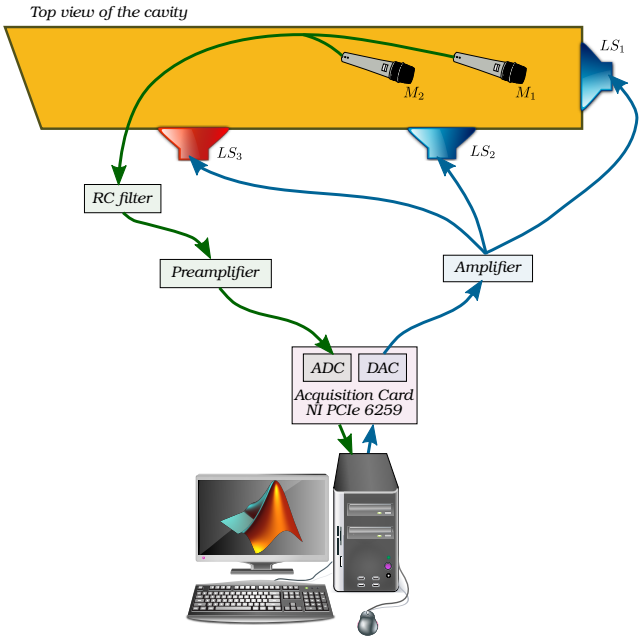

Figure 4: LS2N Box demonstrator

does not contain any passive treatment, the frequency response of the LS2N Box is more complex at high frequency than on the vehicle.

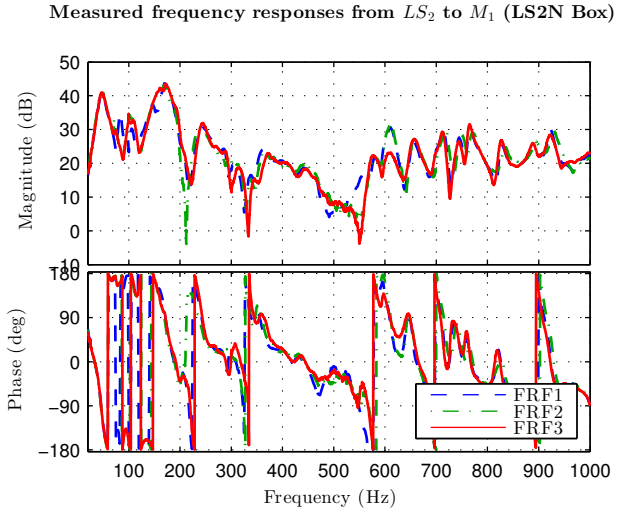

Figure 5: Frequency responses measured on the LS2N Box

The enclosure is instrumented with three loudspeakers and two microphones. Sensors and actuators are connected to the acquisition card through their respective amplifiers. The acquisition card is driven from Simulink through the Real Time Windows Target toolbox of Matlab®. The sampling frequency used is 10 kHz.

In the following, the control loudspeakers are LS_1 and/or LS_2, while LS_3 is used to generate the disturbance. Thus, considering Fig. 3, G_p is the transfer between LS_3 and microphones M_1 and M_2. Even though this transfer is fully

mastered on the prototype, it is considered to be unknown for coherence with the vehicle problem specifications. G_s is the transfer between LS_1 and LS_2 and M_1 and M_2.

The main difference with the vehicle is thus the number of actuators m and sensors l ($m = l = 2$ on the LS2N Box, and $m = 4$, $l = 3$ on the vehicle).

Finally, considering Fig. 5, which depicts the different frequency responses of the same transfer ($LS_2 \rightarrow M_1$) measured in different environment conditions, significant modifications of the magnitude and frequency of the different acoustic modes can be observed. The uncertainties due to the environment conditions must be carefully considered when dealing with the control stage.

3. Indicators

This section describes to the selection of suitable indicators for evaluating the performance and robustness of an ANC solution.

3.1. Performance

In the general ANC problem presented in Fig. 3, the goal of the control is to ensure that the measured signal e remains small compared to the primary noise y_p. The performance may then be evaluated either by considering signals e and y_p and using signal indicators, or by dealing with system indicators based on the transfer $T_{y_p \rightarrow e}$ (which is also the sensitivity function S). These two options are detailed in this section.

3.1.1. Power Spectrum Density (PSD)

Let us first consider the SISO case. In order to evaluate the attenuation obtained by an ANC application, $S_{ee}(j\omega)$ (the PSD of signal e) is generally compared with $S_{y_p y_p}(j\omega)$ (the PSD of y_p) (see for instance [7, 27, 28, 36, 37]). To that end, the following PSD ratio can be calculated:

$$\texttt{PSDR}(j\omega) = \frac{S_{ee}(j\omega)}{S_{y_p y_p}(j\omega)} \tag{1}$$

In the MIMO case, this indicator is applied to each component e_i and y_{p_i} of e and y_p. It then becomes:

$$\texttt{PSDR}_\texttt{i}(j\omega) = \frac{S_{e_i e_i}(j\omega)}{S_{y_{p_i} y_{p_i}}(j\omega)} \tag{2}$$

This informs about the local behavior at each microphone position, but must be completed by an additional indicator in order to evaluate the global performance of the control. It should be noted that, in the SISO case, the indicator PSDR is equivalent to the gain of the transfer $T_{y_p \rightarrow e}$ as it verifies:

$$\texttt{PSDR}(j\omega) = \left| T_{y_p \rightarrow e}(j\omega) \right|^2 \tag{3}$$

In the MIMO case, the link with the gain (or singular value) is no longer direct.

3.1.2. l_2 and power norms

Scalar indicators can be built using norms. Two signal norms may be suitable. Let us consider the l_2 norm of a signal $\|e\|_2$, namely its energy, and its power $\|e\|_{pow}$. Their respective definitions are recalled here [38, 39]:

$$\|e\|_2 = \sqrt{\int_0^\infty \|e(t)\|_2 dt} \tag{4}$$

$$\|e\|_{pow} = \sqrt{\lim_{T \rightarrow \infty} \frac{1}{T} \int_0^T \|e(t)\|_2 dt} \tag{5}$$

Of course, these definitions properly deal with vector signals. To evaluate the performance over a prescribed frequency range, the signal may be weighted with a band-pass filter in order to focus on this range. As for PSD, one may be interested in comparing the signal norms of e and y_p. Such comparisons involve induced norms on transfers, which are introduced in the following.

3.1.3. Singular values

Performance can also be evaluated by considering transfer-based indicators. For example, attenuating e with regard to y_p involves attenuating the transfer that links these two signals. One may then consider the maximal singular value $\bar{\sigma}\left(T_{y_p \rightarrow e}(j\omega)\right)$ of $T_{y_p \rightarrow e}$.

In the SISO case, the singular value is simply the gain in the transfer. As already mentioned, it is equivalent to considering alternatively the gain in $T_{y_p \rightarrow e}$ or the indicator PSDR. In the MIMO case however, there is no direct link between the singular value and the indicator $\texttt{PSDR}_\texttt{i}$. Moreover, while $\texttt{PSDR}_\texttt{i}$ only gives local information, the singular value can be used as an indicator of the global performance of the ANC system.

3.1.4. $\mathcal{H}_2$ and $\mathcal{H}_\infty$ norms

As for signals, norms may be used to obtain scalar indicators. The most suitable ones for ANC applications are $\mathcal{H}_2$ and $\mathcal{H}_\infty$ norms. Their definitions are recalled below [38, 39]:

$$\|T_{y_p \rightarrow e}\|_2 = \sqrt{\frac{1}{2\pi} \int_{-\infty}^{\infty} \text{tr}\left(T^*_{y_p \rightarrow e}(j\omega) T_{y_p \rightarrow e}(j\omega) \right) d\omega} \tag{6}$$

$$\|T_{y_p \rightarrow e}\|_\infty = \sup_\omega \bar{\sigma}(T_{y_p \rightarrow e}(j\omega)) \tag{7}$$

These two norms can be interpreted as induced norms. Table 1 summarizes the link between signal norms and system norms. The $\mathcal{H}_2$ norm can be interpreted as the power of the output signal for a white noise as input. Thus, if a stochastic model of the perturbation y_p is available, the $\mathcal{H}_2$ norm would give a "realistic" evaluation of the attenuation. If such a model is not available, it is better to consider the "worst case" by using the $\mathcal{H}_\infty$ norm. This norm can be interpreted as the ratio between the l_2 norm

$\|y_p\|$	$\|e\|$	$\|T_{y_p \to e}\|$
Energy	Energy	$\mathcal{H}_\infty$
Power	Power	$\mathcal{H}_\infty$
White noise	Power	$\mathcal{H}_2$

Table 1: Induced norms

of the input and the l_2 norm of the output for the worst input case.

Again, if attenuation over a prescribed frequency range is required, a bandpass weighting filter must be used.

However, dealing with the $\mathcal{H}_\infty$ norm leads to considering that the disturbing signal y_p may have completely independent components. This is generally far from reality in an ANC problem. Thus, using $\|T_{y_p \to e}\|_\infty$ as a performance indicator certainly induces pessimism as it prevents the worst input case which never occurs.

An alternative would be to consider $\max_{i,j} \|T_{y_{p_j} \to e_i}\|_\infty$ (where y_{p_j} and e_i are the components of y_p and e, respectively). If this indicator is small, each SISO transfer $T_{y_{p_j} \to e_i}$ will be small, and the triangular equation then shows that it is a sufficient condition to ensure that each signal e_i (and by the way e) has a small l_2 norm whatever the input combination (see third line of equation (8)):

$$\begin{aligned} \|e_i\|_2 &= \|T_{y_{p_1} \to e_i} \times y_{p_1} + \cdots + T_{y_{p_m} \to e_i} \times y_{p_m}\|_2 \\ &\leq \|T_{y_{p_1} \to e_i} \times y_{p_1}\|_2 + \cdots + \|T_{y_{p_m} \to e_i} \times y_{p_m}\|_2 \\ &\leq \|T_{y_{p_1} \to e_i}\|_\infty \|y_{p_1}\|_2 + \cdots + \|T_{y_{p_m} \to e_i}\|_\infty \|y_{p_m}\|_2 \\ &\leq \|T_{y_p \to e}\|_\infty \|y_p\|_2 \end{aligned} \tag{8}$$

Consequently, $\max_{i,j} \|T_{y_{p_j} \to e_i}\|_\infty < \gamma$ is easier to obtain than $\|T_{y_p \to e}\|_\infty < \gamma$, while being a sufficient condition. The indicator $\max_{i,j} \|T_{y_{p_j} \to e_i}\|_\infty$ should be preferred if using the $\mathcal{H}_\infty$ norm.

3.2. Robustness

Two robustness issues must be considered: robustness against neglected dynamics and uncertainties in the control bandwidth.

3.2.1. Neglected dynamics

Acoustic systems generally have a wide bandwidth with numerous resonant modes. Acoustic models used for ANC necessarily have a limited validity range and so neglect some high frequency dynamics. ANC designers must thus ensure that the control has no action outside the validity frequency range of the model. In other words, $u = u_s$ must be small faced with y_p above the validity range of the model. Then three indicators can be considered to evaluate the robustness to neglected dynamics:

- the PSD of u_s: $S_{u_s u_s}$
- the l_2 norm of u_s: $\|u_s\|_2$
- the $\mathcal{H}_\infty$ norm of the control sensitivity KS: $\|KS\|_\infty = \|T_{y_p \to u_s}\|_\infty$.

The two latter indicators must be used with a suitable weighting that penalizes the indicator at frequencies where the model is not valid.

3.2.2. Uncertainties

The second robustness issue concerns the model uncertainties in the control bandwidth. As highlighted in Fig. 5, environment conditions have a significant impact on acoustic transfers. For instance, in a car cabin, temperature, vehicle load, seat positions, number of passengers, *etc.* are parameters that strongly influence the acoustic field. The modulus margin M_m is a possible indicator to evaluate the robustness with regard to such uncertainties. Its definition is recalled here:

$$M_m = \|S\|_\infty^{-1} = \|T_{y_p \to e}\|_\infty^{-1} \tag{9}$$

In ANC applications, this indicator can also be considered an indicator of spatial robustness. In fact, a displacement around a control point induces a variation in gain and phase with regard to the considered transfer. The modulus margin is a guarantee of robustness to simultaneous gain and phase variations.

3.2.3. Multi-model

In the present ANC application, considering only the modulus margin is not enough to handle uncertainties properly. Additional robustness guarantees are mandatory. Uncertainties can be handled in three different ways, one can consider:

- parametric uncertainty;
- unstructured uncertainty;
- a multi-model approach.

The two former approaches are not considered here, mainly because their application may induce some conservatism, which would not be coherent with the objective of precisely evaluating achievable performances. The multi-model approach, which ensures stability and performance for a set of models (not only the nominal one) reflecting some more or less extreme operating conditions, is preferred here, although it potentially leads to necessary conditions only.

4. MIMO identification

In addition to finding a model that reproduces the system behavior over a large frequency range, the objective of this identification stage is to find a minimal MIMO realization that takes advantage of the fact that the different acoustic transfers share the same modes. As explained in the introduction, the subspace approach in the frequency domain [23, 24] was found to be a suitable way to address this identification problem. Other approaches were tested, but gave unsuccessful or similar results.

4.1. LS2N Box demonstrator

Direct MIMO identification was performed on the LS2N Box. The fit values obtained with a model of order 80 are given in Table 2. The definition of the classic fit indicator used is:

$$fit = 100\left(1 - \frac{\|H(.) - \hat{H}(.)\|_2}{\|H(.) - \overline{H}(.)\|_2}\right)$$

where $H(j\omega)$ is the measured frequency response of the system, $\hat{H}(j\omega)$ is the model frequency response and $\overline{H}(j\omega)$ is the mean of $H(j\omega)$ over ω.

fit	$\mathbf{LS_1}$	$\mathbf{LS_2}$
$\mathbf{M_1}$	83.8629	85.0307
$\mathbf{M_2}$	86.8096	90.5583

Table 2: Fit indicator of the MIMO model of the LS2N Box

Fig. 6 compares the model and the measured frequency response for the transfer between LS_1 and M_1 for which the worst fit value was obtained.

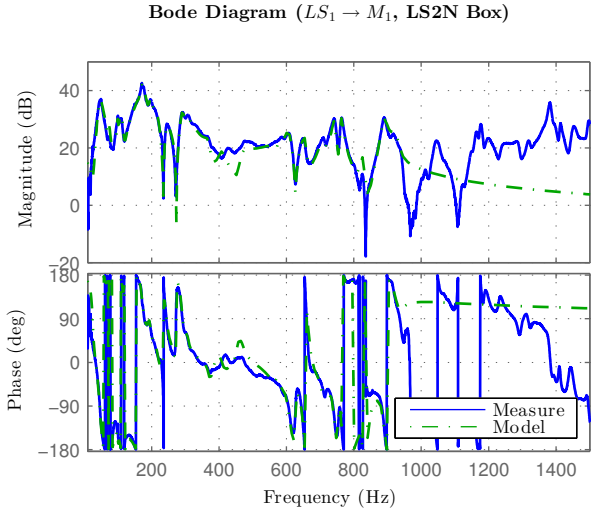

Figure 6: Comparison between the identified model and the measured frequency response (transfer $LS_1 \rightarrow M_1$, LS2N Box)

4.2. Vehicle demonstrator

Direct MIMO frequency identification from vehicle data was unsuccessful. As highlighted in Fig. 2 and discussed in Section 2.2, this difficulty was attributed to the differences in magnitude level observed between the different transfers of the secondary path. Currently, this is still an open problem requiring additional investigation. In the present paper, it was overcome by proceeding indirectly. Each SISO transfer was identified separately and concatenated in a MIMO model. This MIMO model was then reduced using balanced truncation (see for example [38]), to remove duplicated dynamics (shared acoustic modes).

Table 3 contains the order of the different SISO models.

order	$\mathbf{LS_1}$	$\mathbf{LS_2}$	$\mathbf{LS_3}$	$\mathbf{LS_4}$
$\mathbf{M_1}$	70	35	30	70
$\mathbf{M_2}$	80	70	40	70
$\mathbf{M_3}$	60	60	70	30

Table 3: Order of SISO models

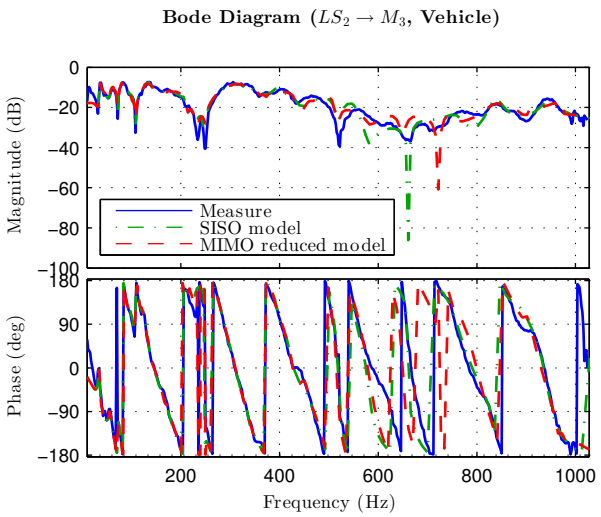

Figure 7: Comparison between the identified models and the measured frequency response (transfer $LS_2 \rightarrow M_3$, Vehicle)

Concatenation of these SISO models leads to a MIMO model of order 685. Reduction leads to a MIMO model of order $n = 158$. Fit values obtained on the reduced model are given in Table 4. (Order reduction was stopped before it had a significant impact on identification.)

fit	$\mathbf{LS_1}$	$\mathbf{LS_2}$	$\mathbf{LS_3}$	$\mathbf{LS_4}$
$\mathbf{M_1}$	88.3293	76.9562	84.1409	80.7295
$\mathbf{M_2}$	83.8304	85.7894	79.1181	83.7762
$\mathbf{M_3}$	81.1993	74.3320	91.0322	88.5743

Table 4: Fit indicator of the MIMO reduced order model

Fig. 7 compares the model and the measured frequency response for the transfer between LS_2 and M_3 for which the worst fit value was obtained after model reduction. It clearly shows that the identification/reduction leads to a suitable model, at least up to 500 Hz.

5. Multi-objective control

The proposed control methodology was developed in order to evaluate achievable performances precisely. It makes use of the indicators presented in Section 3 to formalize the specifications.

5.1. Performance

As already mentioned, the controller must ensure the smallness of the norm of the transfer $T_{y_p \rightarrow e} = S$ over a predetermined frequency range. As no *a priori* exploitable

information is available concerning the disturbance y_p, a worst case approach is chosen using the $\mathcal{H}_\infty$ norm:

$$\min_{K\in\mathcal{K}} \max_{i,j} \|W_1 T_{y_{p_j}\to e_i}\|_\infty \tag{10}$$

where W_1 is a bandpass filter on $[f_{min}, f_{max}]$, K is the sought controller and $\mathcal{K} \subset \mathcal{RH}_\infty$ is the controller space.

5.2. Robustness

The first robustness constraint deals with the high frequency dynamics neglected by the model. It ensures that the controller has no action outside the validity frequency range of the model: [20, 1000] Hz:

$$\|W_2 T_{y_p\to u_s}\|_\infty < 1 \tag{11}$$

In this inequality, the weighting transfer W_2 is chosen to penalize the control sensitivity function $KS = T_{y_p\to u_s}$ at frequencies above 1000 Hz.

The second constraint of robustness imposes a minimal modulus margin:

$$\|T_{y_p\to e}\|_\infty^{-1} = \|S\|_\infty^{-1} > W_3 \tag{12}$$

where W_3 is a constant in $[0, 1]$.

5.3. Controller dynamics

Two additional constraints on the controller dynamics are introduced. First, the controller K must be stable as it belongs to $\mathcal{K}$, which is a subset of $\mathcal{RH}_\infty$. So, strong stability is imposed. This avoids potential difficulties when implementing the controller. Furthermore, in the case of feedback control, the presence of unstable poles in the loop transfer amplifies the waterbed effect and so must be avoided. The constraint is formalized as follows:

$$Re\left(p_{r_K}\right) < -\epsilon \tag{13}$$

where p_{r_K} designates the r^{th} controller pole with $1 \le r \le n_K$ (n_K being the controller order).

The second constraint prevents difficulties during the discretization stage, by imposing the controller poles to comply with:

$$|p_{r_K}| < \frac{2\pi f_e}{N_f} \tag{14}$$

In this expression, f_e is the sampling frequency, $N_f \ge 2$.

5.4. Control problem

The control problem derived from the specifications is summarized as:

$$\min_{K\in\mathcal{K}} \max_{k\in\{1,\dots,N\}} \max_{i,j} \left\| W_1 T^{(k)}_{y_{p_j}\to e_i} \right\|_\infty \tag{15}$$

with:

$$\begin{cases} \max_{k\in\{1,\dots,N\}} \left\| W_2 T^{(k)}_{y_p\to u_s} \right\|_\infty < 1 \\ \max_{k\in\{1,\dots,N\}} \left\| W_3 T^{(k)}_{y_p\to e} \right\|_\infty < 1 \\ Re\left(p_{r_K}\right) < -\epsilon \\ |p_{r_K}| < \frac{2\pi f_e}{N_f} \end{cases} \tag{16}$$

In these expressions, $T^{(k)}_{y_{p_j}\to e_i}$ denotes the closed-loop transfer $T_{y_{p_j}\to e_i}$ obtained for the k$^{\text{th}}$ plant model. This is the formalization of the multi-model approach discussed in section 3.2.3.

The associated augmented model is given in Fig. 8.

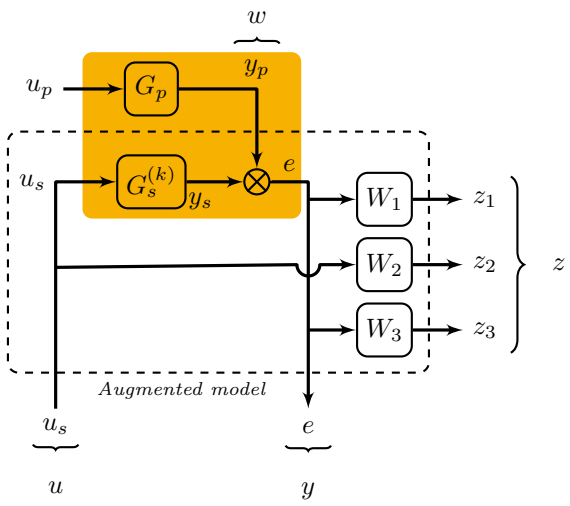

Figure 8: Control problem formulation

5.5. Non-smooth optimization

The control problem described above is MIMO, multi-objective and multi-model. This makes the optimization problem non-convex and non-smooth. Even in the case where it could be relaxed without too much conservatism as a convex optimization problem (which is not the case), it would be hardly tractable due to the high order of the models and controller involved.

According to the authors, a suitable way to address such an optimization problem is to consider direct (and consequently) non smooth optimization. In control, this approach was initiated by Pierre Apkarian and Dominikus Noll in [40, 41, 42], with the `systune` solver [43] on one hand and by Michael Overton, Didier Henrion, Denis Arzelier and co-authors with the HIFOO solver [44, 45] on the other hand. Despite the fact that both solvers optimize in the controller space, they have little in common in terms of algorithms. The differences are not detailed in this paper; the reader may refer to the review [46].

In the following, the results were obtained using the `systune` (Matlab R2014a) solver.

5.6. An observer-based controller structure

The observer-state feedback structure is considered to parameterize admissible stable and stabilizing controllers. It is derived in (18) from the state-space model of G_s (17).

$$\begin{cases} \dot{x}_s = A_s x_s + B_s u_s \\ y_s = C_s x_s + D_s u_s \end{cases} \tag{17}$$

$$\begin{cases} \dot{\hat{x}}_s = A_s \hat{x}_s + B_s u_s + K_f(e - \hat{y}_s) \\ \hat{y}_s = C_s \hat{x}_s + D_s u_s \\ u_s = -K_c \hat{x}_s \end{cases} \tag{18}$$

The only free parameters are the state feedback and observer gains: K_c and K_f. Hence, since the controller and the model are of the same order ($n_K = n$), the proposed observer-based controller leads to $n \times (m+l)$ decision variables only, while a full-order controller would involve $n^2 + n \times (m + l) + m \times l$ decision variables.

5.7. Initialization

The initial controller is chosen as the solution of the standard $\mathcal{H}_2$/LQG control problem presented in Fig. 9.

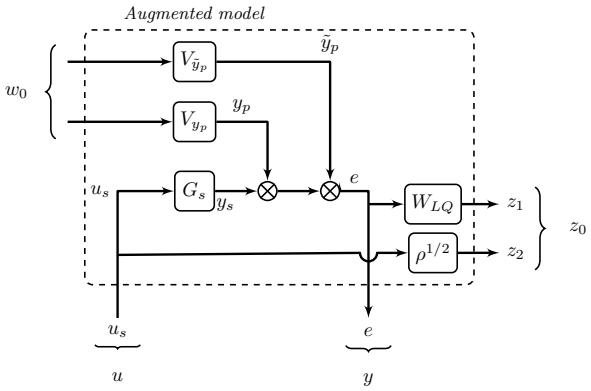

Figure 9: $\mathcal{H}_2$/LQG initialization

In this initial control problem, W_{LQ} is a bandpass filter that controls the attenuation frequency range, whereas ρ manages the trade-off between performance and control energy. $V_{\tilde{y}_p}$ and V_{y_p} are the covariance matrices of output noises, separated into $\tilde{y}_p$ and y_p assuming they are sensor and disturbing noises, respectively.

This $\mathcal{H}_2$/LQG controller is designed to be a feasible point with regard to the multi-objective control problem. To that end, parameter ρ is tuned to favor the control energy-saving rather than the performances.

An $\mathcal{H}_2$/LQG initialization is preferred to a standard $\mathcal{H}_\infty$ one, mainly because it does not involve undesirable coupling between transfers, it is simpler to tune and the resulting controller has the appropriate structure.

6. Simulation and experimental results

The control methodology was applied to both experimental platforms in simulations. Experimental validation was conducted only on the LS2N Box. The multi-model approach was applied only on the LS2N Box. It should be noted that the values of criterion (15) given in the following are normalized (by definition), *i.e.* attenuation is obtained over the desired range if the criterion is less than 1.

6.1. Low frequency attenuation

Let us first consider low frequency attenuation (*i.e.* below 100 Hz). The criterion values obtained are given in Table 5 (see (15) for the expression of the criterion). On

	LS2N Box	Vehicle
50-80 Hz	0.47	0.27

Table 5: Low frequency criteria

both demonstrators, significant attenuation is obtained at low frequency. This result is consistent with our expectations for the LS2N Box, in which the loudspeakers are not equipped with a back enclosure and so can work even at low frequencies. On the vehicle, limitations were expected to be greater at low frequency as some transfers have a very low gain. The results show that this is not the case. The criterion values are confirmed by the singular value of the corresponding transfer presented in Fig. 10 and Fig. 11 for the LS2N Box and the vehicle, respectively.

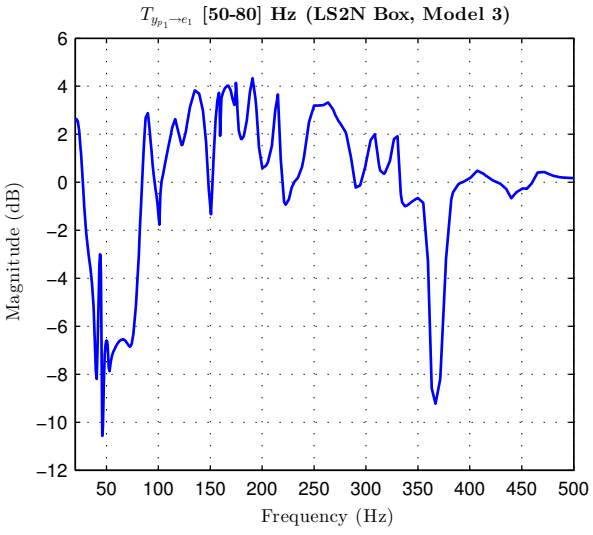

Figure 10: Magnitude of the transfer $T_{y_{p_1} \to e_1}$ (Model 3) in the LS2N Box (attenuation range [50-80] Hz, simulation)

The amplification observed outside the attenuation range is an illustration of the waterbed effect.

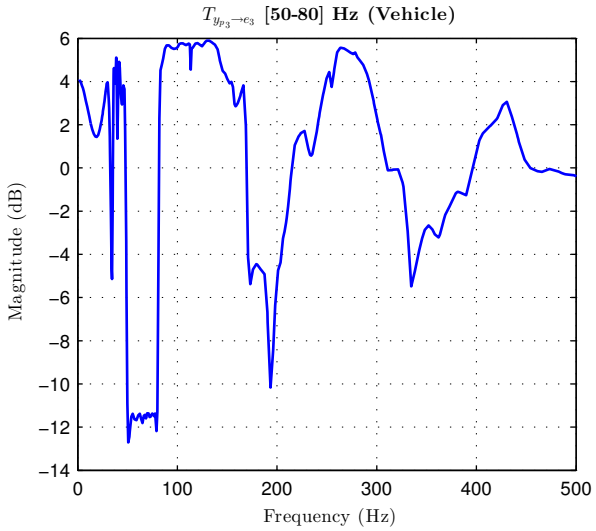

Figure 11: Magnitude of the transfer $T_{y_{p_3}\to e_3}$ in the vehicle (attenuation range [50-80] Hz, simulation)

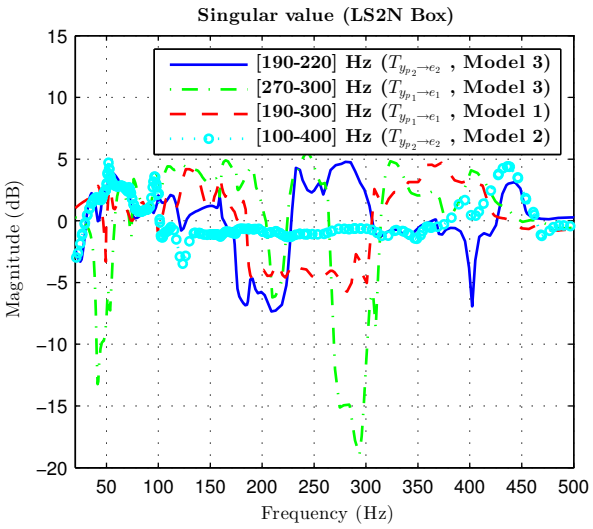

Figure 12: Magnitude of the transfer associated with the criterion value of Table 6 (LS2N Box, Simulation)

6.2. Attenuation level vs. frequency range width

A second important question regarding performances concerns the attenuation achievable with respect to the width of the chosen frequency range. Of course, when the width of the attenuation range increases, the attenuation level is expected to decrease. The goal of this section is to quantify this phenomenon, and to see whether broadband attenuation is achievable. To that end, four attenuation ranges are considered; the criterion value of each range is summarized in Table 6.

Frequency range (Hz)	190-220	270-300	190-300	100-400
LS2N Box	0.5150	0.1851	0.6711	0.9303
Vehicle	0.1628	0.1818	0.8354	1

Table 6: Criteria table

The corresponding singular values are given in Fig. 12 and Fig 13 for the LS2N Box and the vehicle, respectively.

A significant attenuation is obtained up to the range 190-300 Hz. Then, for 100-400 Hz no attenuation is observed. It should be noted that the results presented here have been improved with regard to those described in [15]. This is due in particular to the modification of the industrial specifications as the high frequency uncertainties were found to be over-estimated.

6.3. Simulation with experimental noises (vehicle)

In the vehicle case, some additional simulations with experimental measurements of road noise recorded on the vehicle demonstrator are provided. Fig. 14 presents the $\texttt{PSDR}_\texttt{i}$ indicator (2) obtained for the attenuation range [190-220] Hz at each microphone position (M_1 to M_3) while simulating the closed-loop with an experimental road noise measurement as the disturbance (y_p). The level of

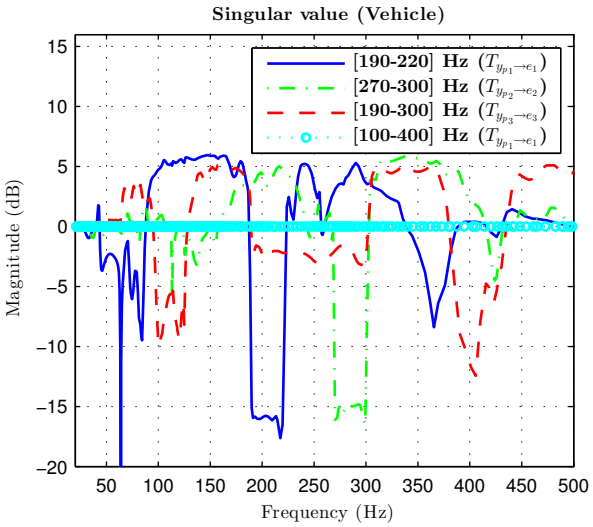

Figure 13: Magnitude of the transfer associated with the criterion value of Table 6 (Vehicle, Simulation)

attenuation is coherent with the solid line (blue) of Fig. 13.

However, care should be taken when comparing the $\texttt{PSDR}_\texttt{i}$ indicator with the singular value one (see Section 3.1.3). As explained in Section 3.1.1, the link between these two indicators is not direct in the MIMO case. The main reason for this is the influence of cross PSD terms on the $\texttt{PSDR}_\texttt{i}$ indicator. When the attenuation obtained on the singular value is significant as in Fig. 13 (solid (blue) line [190-220] Hz), this influence is rather small and thus the attenuation levels of Fig. 13 (solid (blue) line [190-220] Hz) and Fig. 14 seem fully coherent. For smaller attenuation on the singular value indicator, as for instance in Fig. 11 (low frequency attenuation [50-80] Hz), the influence of cross PSD terms increases and differences between the $\texttt{PSDR}_\texttt{i}$ indica-

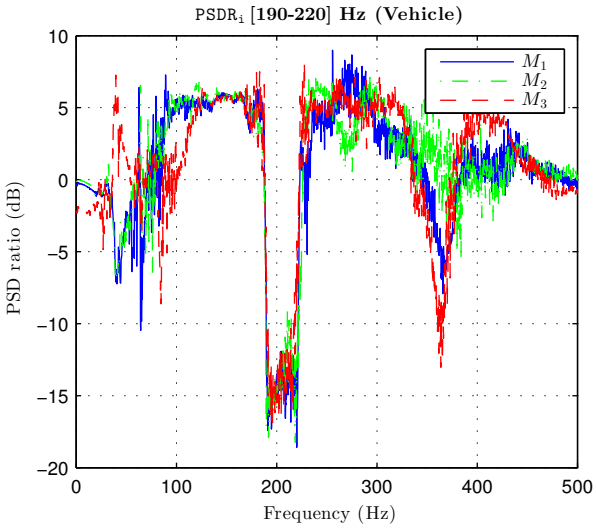

Figure 14: PSDR$_i$ (attenuation range [190-220] Hz) Vehicle, Simulation

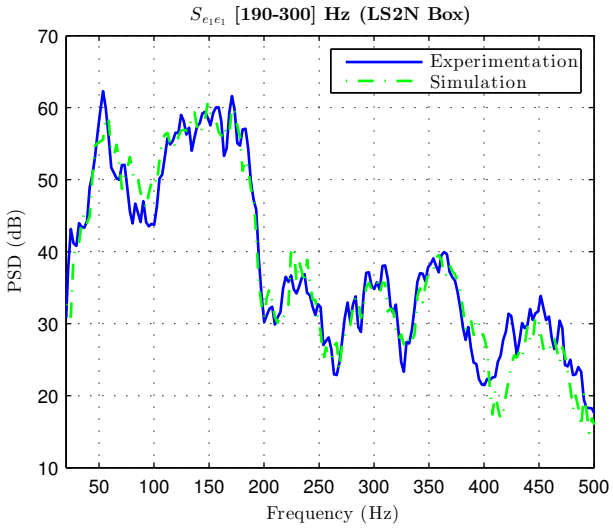

Figure 16: Closed-loop spectrum of microphones signals

tor and the singular value may appear (compare Fig. 11 with Fig. 15, lines M_1 and M_2).

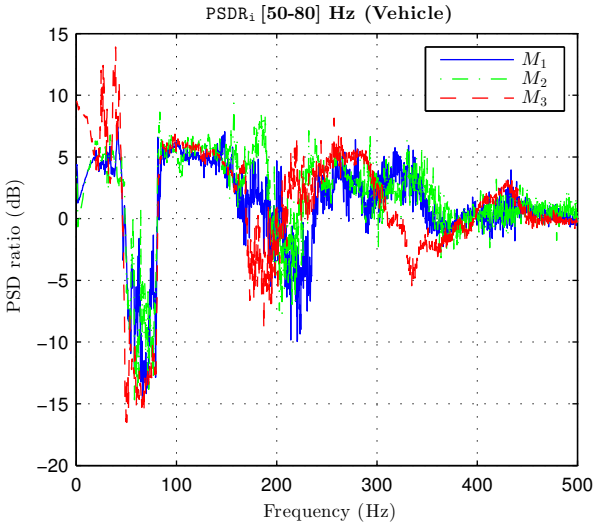

Figure 15: PSDR$_i$ (attenuation range [50-80] Hz) Vehicle, Simulation

6.4. Experimental validations (LS2N Box)

The results described above were obtained in simulations. Those obtained on the LS2N Box were validated experimentally. Fig. 16 compares the power spectrum density $S_{e_1e_1}$ of signal e_1 obtained (in a closed-loop) in a simulation and experimentally. As for the other ranges, there is good agreement between the simulation and the experimental results.

6.5. Attenuation at non-control points (LS2N Box)

The control strategy presented above was designed to obtain attenuation only at the control microphone positions. Further investigation would be needed to propose a control strategy that ensures global attenuation in the cavity. However, the results obtained at non-control points may be interesting to see whether the presented strategy achieves some spatial attenuation. Fig. 18 presents the attenuation obtained experimentally on the LS2N Box on a microphone M_3 placed at a non-control point (see Fig. 17). Three attenuation ranges were considered: 50-80 Hz, 190-220 Hz and 270-300 Hz. Over two ranges (50-80 Hz and 270-300 Hz), some attenuation is obtained at the considered non-control point whereas no attenuation occurs at 190-220 Hz. Similar results were obtained on microphone M_4. Thus, the control strategy may achieve attenuation at non-control points but no guarantee is given. This is an encouraging result for readers interested in spatial attenuation.

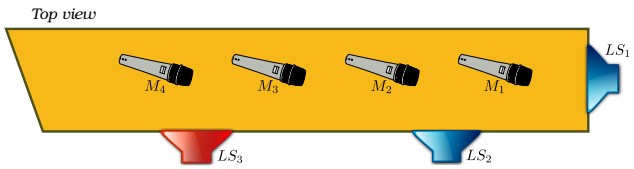

Figure 17: Position of microphones M_3 and M_4 (non-control points)

7. Conclusions

In this paper, a complete methodology is proposed to evaluate numerically the achievable performances in the problem of broadband ANC in a car cabin. The contributions of the paper are threefold.

First, a detailed presentation of signal- and transfer-based indicators for the evaluation of the performance and robustness of ANC applications is given. Some of these indicators, adapted from the robust control theory, are new in the context of ANC. All these indicators enable the control specifications to be formalized as a multi-objective

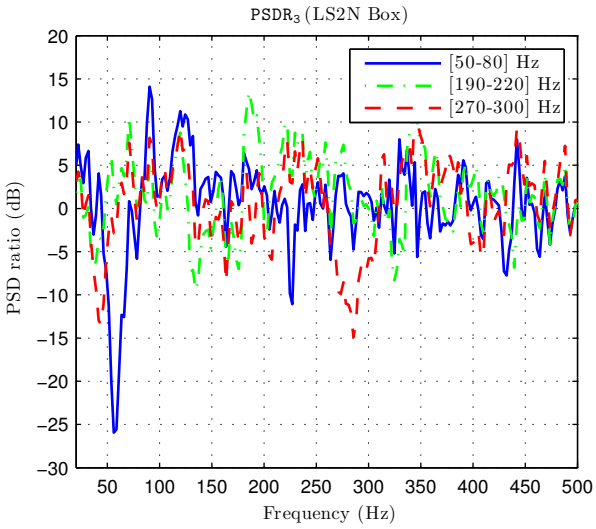

Figure 18: Attenuation on microphone M_3 (non-control point)

optimization problem, with as little pessimism as possible, and thus make possible a precise evaluation of achievable performances.

Secondly, the paper proposes a coherent methodology to evaluate the achievable performances for the considered ANC problem. The main industrial constraint consisted of using the actuators and sensors available on serial cars and used for engine noise reduction. As there is no measure available for feedforward compensation, a pure feedback control strategy is considered. The achievable performances are discussed depending on low frequency attenuation and the width of the attenuation range. The methodology used and the results obtained are a valuable decision-making tool when questioning the potential of a given ANC architecture.

The third contribution lies in the results obtained experimentally, first with the LS2N Box (developed specifically for the study and used for early investigation), and secondly with the vehicle prototype. There is good agreement between the simulation and the experimentation. These results lead to the conclusion that robust broadband attenuation (by feedback) is achievable in the considered control problem and enables road noise attenuation. Despite the so-called waterbed effect inherent in the feedback control scheme, a good level of attenuation is obtained over ranges of 30 Hz width. Attenuation is still significant over ranges of 110 Hz but it is almost nonexistent over ranges of 300 Hz.

Finally, the results and limitations observed constitute an interesting basis to develop the next generation of ANC architecture in cars, with spatial attenuation aspects as a perspective.

Acknowledgements

The authors wish to thank the car manufacturer Renault for its financial support during this work.

References

[1] H. Coanda, Procédé de protection contre les bruits (1930).
[2] P. Lueg, Process of silencing sound oscillations (1936).
[3] R. S. Pea, M. Cuguer, A. Masip, J. Quevedo, V. Puig, Robust identification and feedback design: An active noise control case study, Control Engineering Practice 16 (11) (2008) 1265 – 1274. doi:http://dx.doi.org/10.1016/j.conengprac.2008.02.004.
[4] A. J. Hull, C. J. Radcliffe, S. C. Southward, Global active noise control of a one-dimensional acoustic duct using a feedback controller, Journal of Dynamic Systems, Measurement, and Control 115 (3) (1993) 488–494.
[5] O. Kaiser, R. Pfiffner, M. V. Kothare, F. J. Kraus, C. Rhodes, M. Morari, Modeling and Robust Control of Active Noise Control Systems, in: Conference on Decision and Control, Kobe, Japan, 1996, pp. 283–291.
[6] J. C. Carmona, V. M. Alvarado, Active Noise Control of a Duct Using Robust Control Theory, IEEE Transactions on Control Systems Technology 8 (6) (2000) 930–938.
[7] B. Rafaely, S. J. Elliott, $\mathcal{H}_2/\mathcal{H}_\infty$ Active Control of Sound in a Headrest: Design and Implementation, IEEE Transactions on Control Systems Technology 7 (1) (1999) 79–84.
[8] M. Pawelczyk, Adaptive noise control algorithms for active headrest system, Control Engineering Practice 12 (9) (2004) 1101 – 1112. doi:http://dx.doi.org/10.1016/j.conengprac.2003.11.006.
[9] D. P. Das, D. J. Moreau, B. S. Cazzolato, Nonlinear active noise control for headrest using virtual microphone control, Control Engineering Practice 21 (4) (2013) 544 – 555. doi:http://dx.doi.org/10.1016/j.conengprac.2012.11.007.
[10] R. Schirmacher, R. Hunkel, M. Burghardt, Active Noise Control for the 4.0 TFSI with cylinder on Demand Technology in Audi's S-Series, SAE International.
[11] B. Vau, Method and device for narrow-band noise suppression in a vehicle passenger compartment (2009).
[12] J. Cheer, Active control of the acoustic environment in an automobile cabin, Ph.D. thesis, University of Southampton, Southampton (2012).
[13] P. Loiseau, P. Chevrel, M. Yagoubi, J.-M. Duffal, Broadband Active Noise Control Design through Nonsmooth $\mathcal{H}_\infty$ Synthesis, in: IFAC Symposium on RObust CONtrol Design (ROCOND), Bratislava, Slovak Republic, 2015, pp. 395–400.
[14] P. Loiseau, P. Chevrel, M. Yagoubi, J.-M. Duffal, $\mathcal{H}_\infty$ Multi-objective and Multi-model MIMO control design for Broadband noise attenuation in an enclosure, in: European Control Conference, Aalborg, Denmark, 2016, pp. 643–648.
[15] P. Loiseau, P. Chevrel, M. Yagoubi, J.-M. Duffal, A robust feedback control design for broadband noise attenuation in a car cabin, in: IFAC World Congress, Toulouse, France, 2017, pp. 2823–2830.
[16] B. Fang, A. Kelkar, S. Joshi, H.R.Pota, Modelling, system identification, and control of acoustic-structure dynamics in 3-D enclosures, Control Engineering Practice 12 (8) (2004) 989–1004.
[17] S. J. Elliott, Signal Processing for Active Control, in: R. Green, T. Nguyen (Eds.), Signal Processing and its Applications, Academic Press, London, 2001, p. 511.
[18] L. Ljung, System Identification Theory for the User, in: T. Kailath (Ed.), Prentice Hall Information and System Sciences Series, 2nd Edition, Prentice-Hall PTR, Upper Saddle River, New Jersey, 1999, p. 609.
[19] I. R. Petersen, H. Pota, Experiments in Feedback Control of an Acoustic Duct, in: Conference on Control Applications, Anchorage, Alaska, USA, 2000, pp. 261–266.
[20] T. McKelvey, A. Fleming, S. R. Moheimani, Subspace-based system identification for an acoustic enclosure, in: Conference on Control Applications, Anchorage, Alaska, USA, 2000, pp. 255–260.
[21] R. O'Brien, Jr, J. Watkins, G. Piper, D. Baumann, $\mathcal{H}_\infty$ Active Noise Control Of Fan Noise In An Acoustic Duct, in: American Control Conference, Chicago, Illinois, USA, 2000, pp. 3028–3032.

[22] H. Pota, I. R. Petersen, A. G. Kelkar, Robust control of a 2D acoustic duct, in: IFAC 15th Triennial World Congress, Barcelona, Spain, 2002, pp. 67–72.
[23] T. McKelvey, Subspace Methods for Frequency Domain Data, in: American Control Conference, Boston, Massachusetts, 2004, pp. 673–678.
[24] P. V. Overschee, B. D. Moor, Continuous-time frequency domain subspace system identification, Signal Processing 52 (2) (1996) 179–194.
[25] S. Lefteriu, A. C. Ionita, A. C. Antoulas, Modeling Systems Based on Noisy Frequency and Time Domain Measurements, Springer Berlin Heidelberg, Berlin, Heidelberg, 2010, pp. 365–378.
URL https://doi.org/10.1007/978-3-540-93918-4_33
[26] S. J. Elliott, I. M. Stothers, P. A. Nelson, A Multiple Error LMS Algorithm and Its Application to the Active Control of Sound and Vibration, IEEE Transactions on Acoustics, Speech and Signal Processing ASSP-35 (10) (1987) 1423–1434.
[27] T. Sutton, S. J. Elliott, M. McDonald, T. Saunders, Active control of road noise inside vehicles, Noise Control Engineering Journal 42 (4) (1994) 137–147.
[28] H. Sano, T. Inoue, A. Takahashi, K. Terai, Y. Nakamura, Active Control System for Low-Frequency Road Noise Combined With an Audio System, IEEE Transactions on Speech and Audio Processing 9 (7) (2001) 755–763.
[29] C. Boultifat, P. Loiseau, P. Chevrel, J. Lohéac, M. Yagoubi, FxLMS versus $\mathcal{H}_\infty$ Control for Broadband Acoustic Noise Attenuation in a Cavity, in: IFAC World Congress, Toulouse, France, July 9-14, 2017, pp. 9614–9620.
[30] I. R. Petersen, Multivariable control of noise in an acoustic duct, in: European Control Conference, Porto, Portugal, 2001, pp. 414–419.
[31] F. Liu, B. Fang, A. G. Kelkar, LQG-Based Robust Control of Acoustic-Structure Interaction in 3-D Enclosure, in: American Control Conference, Denver, Colorado, USA, 2003, pp. 803–808.
[32] X. H. Yang, J. van Niekerk, K. S. Parwani, A. Packard, B. Tongue, Attenuation of Structurally Generated Interior Noise Through Active Control, in: American Control Conference, San Francisco, CA, 1993, pp. 1–7.
[33] V. Kucera, Factorization of Rational Spectral Matrices: A Survey of Methods, in: IEEE Int. Conf. Control, Edinburgh, U.K., 1991, pp. 1074–1078.
[34] A. H. Sayed, T. Kailath, A survey of spectral factorization methods, Numer. Linear Algebra Appl. 8 (7) (2001) 467–496.
[35] L. L. Beranek, I. L. Ver, Noise and vibration control engineering, Principles and applications, John Wiley and Sons, Inc., New York, 1992.
[36] M. Keller, Contrle actif du bruit basses frquences l'intrieur d'un hlicoptre, Ph.D. thesis, Universit de Provence Aix-Marseille I, Marseille (2008).
[37] S. Berthilsson, A. Barkefors, M. Sternad, MIMO Design of Active Noise Controllers for Car Interiors: Extending the Silenced Region at Higher Frequencies, in: American Control Conference, Fairmont Queen Elizabeth, Montreal, Canada, 2012, pp. 6140–6147.
[38] S. Skogestad, I. Postlethwaite, Multivariable Feedback Control, Analysis and Design, 2nd Edition, John Wiley & Sons, Ltd, England, 2005.
[39] K. Zhou, J. C. Doyle, K. Glover, Robust and Optimal Control, Prentice-Hall, Inc., London, 1996.
[40] P. Apkarian, D. Noll, Nonsmooth $\mathcal{H}_\infty$ Synthesis, IEEE Transactions on Automatic Control 51 (1) (2006) 71–86.
[41] P. Apkarian, D. Noll, Nonsmooth optimization for multidisk $\mathcal{H}_\infty$ synthesis, European Journal of Control 12 (3) (2006) 229–244.
[42] P. Apkarian, D. Noll, A. Rondepierre, Mixed H_2/H_∞ Control via Nonsmooth Optimization, SIAM J. Control and Optimization 47 (3) (2008) 1516–1546.
[43] P. Apkarian, Tuning Controllers Against Multiple Design Requirements, in: American Control Conference (ACC), Washington, 2013, pp. 3888–3893.
[44] S. Gumussoy, D. Henrion, M. Millstone, M. L.Overton, Multiobjective Robust Control with HIFOO 2.0, in: IFAC Symposium on RObust CONtrol Design (ROCOND), Haifa, Israel, 2009.
[45] D. Arzelier, G. Deaconu, S. Gumussoy, D. Henrion, $\mathcal{H}_2$ for HIFOO, in: International Conference on Control and Optimization with Industrial Applications, Bilkent University, Ankara, Turkey, 2011.
[46] M. S. Sadabadi, D. Peaucelle, From static output feedback to structured robust static output feedback: A survey, Annual Reviews in Control (2016) 1–16.